JOURNAL OF GEOPHYSICAL RESEARCH, VOL. 117, A09307, doi:10.1029/2012JA018039, 2012

Anomalously low geomagnetic energy inputs during 2008 solar minimum

Yue Deng,[1] Yanshi Huang,[1] Stan Solomon,[2] Liying Qian,[2] Delores Knipp,[3] Daniel R. Weimer,[4] and Jing-Song Wang[5]

Received 18 June 2012; revised 10 August 2012; accepted 12 August 2012; published 14 September 2012.

[1] The record-low thermospheric density during the last solar minimum has been reported and it has been mainly explained as the consequence of the anomalously low solar extreme ultraviolet (EUV) irradiance. In this study, we examined the variation of the energy budget to the Earth's upper atmosphere during last solar cycle from both solar EUV irradiance and geomagnetic energy, including Joule heating and particle precipitation. The globally integrated solar EUV power was calculated from the EUV flux model for aeronomic calculations (EUVAC) driven by the MgII index. The annal average of solar power in 2008 was 33 GW lower than that in 1996. The decrease of the globally integrated geomagnetic energy from 1996 to 2008 was close to 29 GW including 13 GW for Joule heating from Weimer (2005b) and 16 GW for particle precipitation from NOAA Polar-Orbiting Environmental Satellites (POES) measurements. Although the estimate of the solar EUV power and geomagnetic energy vary from model to model, the reduction of the geomagnetic energy was comparable to the solar EUV power. The Thermosphere Ionosphere Electrodynamic General Circulation Model (TIEGCM) simulations indicate that the solar irradiance and geomagnetic energy variations account for 3/4 and 1/4 of the total neutral density decrease in 2008, respectively.

Citation: Deng, Y., Y. Huang, S. Solomon, L. Qian, D. Knipp, D. R. Weimer, and J.-S. Wang (2012), Anomalously low geomagnetic energy inputs during 2008 solar minimum, *J. Geophys. Res.*, *117*, A09307, doi:10.1029/2012JA018039.

1. Introduction

[2] During the recent extended 23/24 solar cycle minimum, the solar irradiance, activity, and interplanetary magnetic fields had reached levels lower than observed in past minima [*Gibson et al.*, 2011]. Consequently, the lowest observed thermospheric neutral density during 23/24 solar minimum decreased by 29% compared with 22/23 solar minimum after removing the seasonal and geomagnetic activity effects [*Emmert et al.*, 2010; *Emmert and Picone*, 2010]. *Solomon et al.* [2011] reported a 30% decrease in the annual average neutral density from 1996 to 2008. Meanwhile, the global total electron content (TEC) from GPS observations showed a positive trend of 0.6 TEC unit per decade (1 TECU = 10^{16} el m^{-2}) [*Lean et al.*, 2011], while the f_0F_2 from ionosonde data was lower in 23/24 solar minimum than 22/23 at some locations [*Chen et al.*, 2011; *Liu et al.*, 2011].

[3] The record-low thermospheric density and the unusual variation of electron density during last solar minimum have been mainly explained as the consequence of the anomalously low solar extreme ultraviolet (EUV) irradiance [*Emmert et al.*, 2010; *Solomon et al.*, 2010, 2011]. The variation of geomagnetic energy has received relatively less attention or has been treated as negligible [*Solomon et al.*, 2011; *Chen et al.*, 2011]. Actually, it is still in debate if the change of solar EUV irradiance is sufficient to cause the observed variation in the upper atmosphere or not. *Emmert et al.* [2010] showed that about 10% of neutral density difference is attributable to lower solar EUV irradiance and around 16% of the observed density difference remains unexplained. *Solomon et al.* [2011] reported that solar EUV irradiance change alone caused 22% annual average neutral density reduction. They found that combining the solar EUV effect with the geomagnetic energy (2.2%) and CO_2 cooling (3%), totally 27% neutral density decrease can be explained, which is very close to the satellite observed value (30%). However, 15% lower solar irradiance in 2008 than in 1996 can result in a global TEC trend of 3 TECU per decade, which is much larger than the observation and can be implausible [*Lean et al.*, 2011].

[4] The Sun is the ultimate energy source for the upper atmosphere. Typically, the solar EUV irradiance is viewed as the direct solar source of energy deposition and the

[1]Department of Physics, University of Texas at Arlington, Arlington, Texas, USA.
[2]High Altitude Observatory, National Center for Atmospheric Research, Boulder, Colorado, USA.
[3]Aerospace Engineering Sciences, University of Colorado, Boulder, Colorado, USA.
[4]Electrical and Computer Engineering, Virginia Tech Hampton Roads Center, Hampton, Virginia, USA.
[5]China Meteorological Administration, Beijing, China.

Corresponding author: Y. Deng, Department of Physics, University of Texas at Arlington, 502 Yates St., Arlington, TX 76019, USA. (yuedeng@uta.edu)

0148-0227/12/2012JA018039

geomagnetic energy, including both Joule heating and particle precipitation energy, is treated as the indirect solar source, which is transported through the solar wind and magnetosphere [*Knipp et al.*, 2004; *Xu*, 2011]. Given that the solar activity was extremely low in 23/24 solar minimum, both direct and indirect solar sources should vary accordingly and contribute to the change in the upper atmosphere. The globally averaged thermosphere mass density climatologically is a function of both solar irradiation and geomagnetic activity [*Emmert and Picone*, 2010]. The total Joule heating [from *Weimer*, 2005a] model also shows a good correlation with the CHAMP and GRACE satellite measurements [*Weimer et al.*, 2011]. It is very important to know how much energy was reduced in different forms between the last two solar minima, which is critical to explain the unusual variation in the upper atmosphere during 23/24 solar minimum. In this study, we have investigated the variation of the energy budget to the Earth's upper atmosphere from both solar EUV irradiance and geomagnetic energy (Joule heating and particle precipitation) during last solar cycle. Some idealized simulations from Thermosphere Ionosphere Electrodynamic General Circulation Model (TIEGCM) have then been conducted to illustrate their relative roles to the upper thermospheric neutral density variation.

2. Methodology

[5] The EUV flux model for aeronomic calculations (EUVAC) [*Richards et al.*, 1994; *Solomon and Qian*, 2005] has been used to calculate the solar power in the wavelength of 1–105 nm. EUVAC is based on the measured F74113 solar EUV reference spectrum and provides fluxes in the 37 wavelength bins that are in widespread use [*Richards et al.*, 1994]. Individual bands and lines of solar EUV photon flux are calculated from a proxy based on the $F_{10.7}$ index and its 81-day average [*Solomon et al.*, 2011]. $F_{10.7}$ is the index of the 10.7 cm solar radio flux and widely used to represent the solar activity and EUV emissions. But *Solomon et al.* [2011] and *Chen et al.* [2011] reported some issues with $F_{10.7}$ during solar minimum conditions. The MgII core-to-wing ratio (c/w) is a good measure of solar chromospheric activity and a valuable proxy for solar EUV flux [*Solomon et al.*, 2011; *Viereck et al.*, 2004]. After a linear fit of $F_{10.7}$ to MgII c/w, the $M_{10.7}$ index is calculated out from equation (1) in *Solomon et al.* [2011], which is the MgII c/w scaled to $F_{10.7}$ with the unit of 10^{-22} W m^{-2} Hz^{-1}. In this study, the solar EUV flux calculated from EUVAC model with both $F_{10.7}$ and $M_{10.7}$ indices is presented. The total solar EUV power is then estimated through multiplying the solar flux at 1 AU from EUVAC output with the cross section of earth, πR^2, where R is the earth radius and typically set as 6600 km to include the contribution of the atmosphere. The measurements from the Solar EUV Experiment (SEE) [*Woods et al.*, 2005] on the Thermosphere-Ionosphere-Mesosphere Energetics and Dynamics (TIMED) satellite have been compared with the model outputs as well.

[6] Joule heating has been calculated from the *Weimer* [2005a, 2005b] model (W05), the empirical formula [*Foster et al.*, 1983] and the Thermosphere Ionosphere Electrodynamics General Circulation Model (TIEGCM) [*Roble et al.*, 1988; *Richmond et al.*, 1992]. W05 is an empirical model of high-latitude electrodynamics, providing the electric potential, magnetic potential, field-aligned currents and Poynting flux. The downward Poynting flux at the top of ionosphere is obtained from the vector cross product of the electric and perturbation magnetic fields ($S = \frac{\langle \mathbf{E} \times \Delta \mathbf{B} \rangle}{\mu_0}$) [e.g., *Kelley et al.*, 1991; *Gary et al.*, 1995], which supplies one possible way to estimate the height-integrated Joule heating by application of Poynting's theorem [*Kelley et al.*, 1991; *Richmond*, 2010]. The empirical formula ($Q_J(GW) \simeq 4 + 20Kp$) from *Foster et al.* [1983] gives a reasonable description of the single hemisphere Joule heating at the equinoxes for average conditions when Kp < 6. The global Joule heating is close to 2 * Q_J when ignoring the seasonal variations and the interhemispheric asymmetry. TIEGCM is a global first-principle upper atmospheric model, which self-consistently simulates both the neutral and ion species. In the high latitudes, the electric potential pattern is imposed from *Heelis et al.* [1982] empirical model driven by the Kp index and the auroral particle precipitation is specified with the formalism of *Roble and Ridley* [1987] for this study. The Joule heating has been calculated from the localized conductance, ion convection and neutral wind. A factor of 1.5 has been multiplied to the Joule heating to compensate the contribution of the small-scale processes.

[7] The NOAA polar-orbiting operational environmental satellites (POES) continuously monitor the precipitating particles from 50 eV to 20 keV in the polar regions. A technique has been developed to estimate the total particle power deposited in the entire polar region, named as the hemispheric power (HP), from the particle power flux observations along a single satellite pass [*Fuller-Rowell and Evans*, 1987]. The NOAA HP data for each hemisphere during the whole solar cycle are available on the Web site (http://www.swpc.noaa.gov/ftpmenu/lists/hpi.html). The HP of TIEGCM has been calculated from a Kp-dependent empirical formulation based on TIMED/GUVI FUV data [*Zhang and Paxton*, 2008].

3. Results and Discussion

3.1. Solar EUV Irradiance and Geomagnetic Energy Variations

[8] The primary energy sources of the upper atmosphere are the solar EUV irradiance, Joule heating and the particle precipitation. The solar EUV irradiance usually is the largest contributor (80%) to the heating budget, but Joule heating is the most variable one and exceeds the solar EUV irradiance power during some geomagnetic storm periods [*Lu et al.*, 1998; *Knipp et al.*, 2004]. We have examined how the different forms of energy varied between the last two solar minima.

[9] Figure 1 depicts the 81-day centered running mean of the globally integrated solar EUV irradiance and geomagnetic energy during last solar cycle (1995–2009). The yellow shadow regions mark the 22/23 solar minimum in 1996 and 23/24 solar minimum in 2008. The top panel is the solar power in the wavelength of 1–105 nm calculated from EUVAC model driven by the $M_{10.7}$ index. The yearly average of solar power in 2008 was 300.6 GW, which was 33 GW (10%) lower than that in 1996 (333.6 GW). Due to the wavelength dependence of the solar irradiance, the overall percentage reduction in EUV (10%) was lower than that

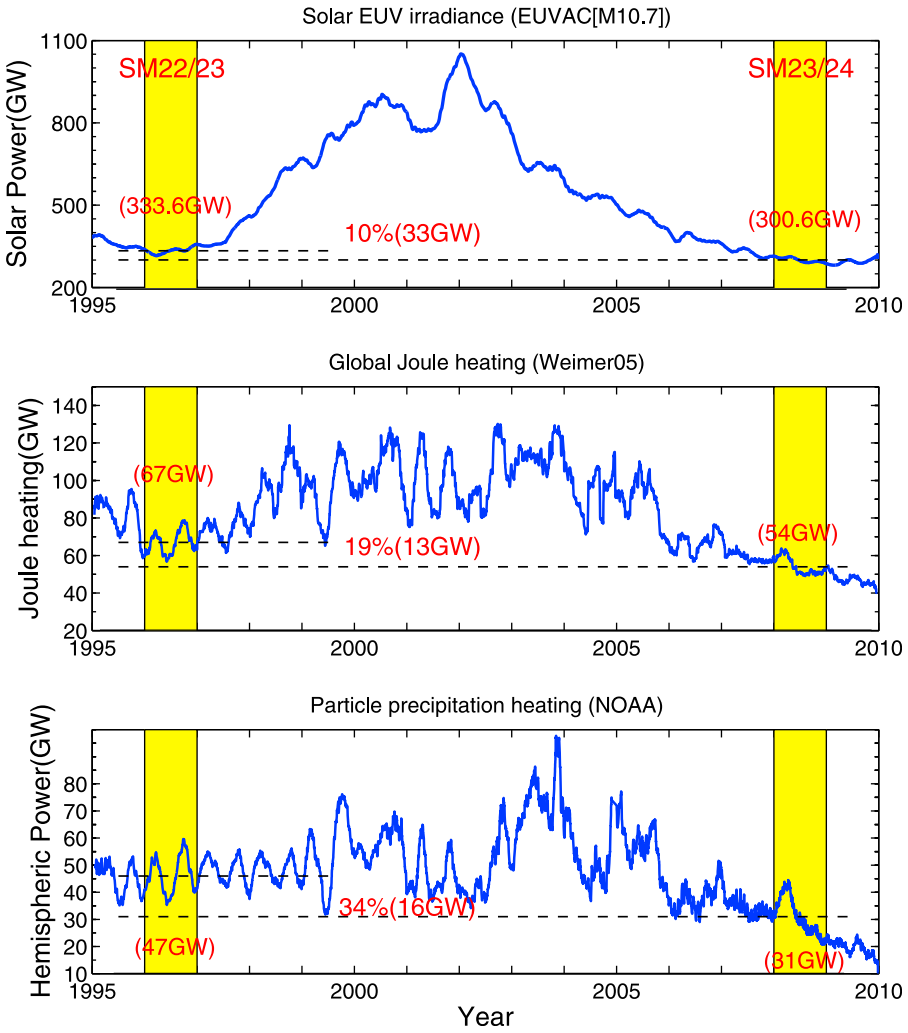

Figure 1. The 81-day running averages of solar EUV irradiance and geomagnetic energy during last solar cycle (1995–2009). The yellow shadow regions mark the 22/23 solar minimum in 1996 and 23/24 solar minimum in 2008. (top) The solar power in the wavelength of 0–105 nm calculated from EUVAC model. (middle) The global integrated Joule heating from W05 empirical model driven by the OMNII solar wind data. (bottom) The global integrated particle precipitation energy from NOAA satellites measurements.

(15%) in the wavelength band of 26–34 nm measured by SOHO/SEM instrument [*Solomon et al.*, 2010]. The middle panel represents the globally integrated Joule heating from W05 empirical model driven by the OMNII hourly solar wind data. The quiet solar wind conditions ($B_y = B_z = 0$, $V_{sw} = 400$ km/s) have been filled in when there is a data gap in the OMNII data. The typical W05 output is a polar distribution of altitudinally integrated Joule heating in the northern hemisphere. To cover the southern hemisphere, W05 was run with the same solar wind conditions but a flipped B_y value and a flipped dipole tilt angle, in which the inter-hemispheric asymmetry has been neglected. As illustrated in Figure 1, the globally integrated Joule heating was reduced by 13 GW (19%) from 1996 (67 GW) to 2008 (54 GW). The bottom panel shows that the globally integrated particle precipitation energy from NOAA satellites also decreased by 16 GW (34%) in 2008. The total geomagnetic energy, including both Joule heating and particle precipitation energy, decreased by 29 GW (13 GW + 16 GW), which was comparable with the reduction of the solar power (33 GW). It suggests that the contribution of geomagnetic energy variation to the neutral density reduction may not be negligible.

[10] Figure 2 compares the annual averages of the global integrated Joule heating to the annual averages of the solar power from the EUVAC model driven by the $M_{10.7}$ index in both ascending and descending phases of the solar cycle. Clearly, both Joule heating and solar power in 2008 and 2009 were lower than those in 1996. The best linear fit is shown in magenta for ascending and light blue for descending. Since the large variation of Joule heating caused by the geomagnetic storms during solar maximum is out of the scope of this study, the points for the annual averages in 2000–2002 have been dropped out. In the ascending phase the slope was close to 0.07, which means the Joule heating increased by 0.07 GW

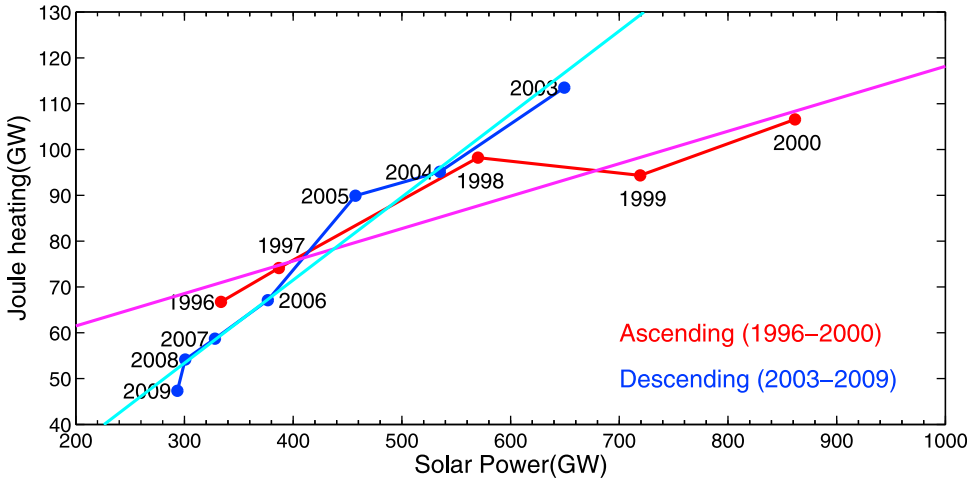

Figure 2. Comparison of global integrated Joule heating annual averages to solar EUV power annual averages during solar cycle 23. Red lines, ascending phase (1996–2000); blue lines, descending phase (2003–2009). The magenta and light blue lines are the best linear fits for the ascending and descending phases.

for every 1 GW enhancement of the solar power. The slope for the descending phase was close to 0.18, which is more than two times higher than that for the ascending phase. In other words, the Joule heating changed relatively faster in the descending phase than the ascending phase. For example, from 1996 to 1997, the solar power and Joule heating increased by 53.3 GW and 5.4 GW, respectively. From 2008 to 2009, the solar power and Joule heating decreased by 7.1 GW and 6.8 GW, respectively. The variation of Joule heating was comparable with the variation of solar power from 2008 to 2009, while the variation of solar power was dominant in the total energy change from 1996 to 1997. Therefore, the contribution of Joule heating variation to the total energy change in the descending phase was more significant than in the ascending phase.

3.2. Comparison of Energy Estimations From Different Sources

[11] The energy estimation uncertainty is one of the biggest problems in the upper atmosphere simulation. The solar power and Joule heating calculated from different models have therefore been compared in this section. Figure 3 shows the variation of solar power from EUVAC model and TIMED/SEE measurements during last solar cycle. The integrated EUV energy flux is derived from the EUVAC model using either $M_{10.7}$ or $F_{10.7}$ as input. The energy flux is

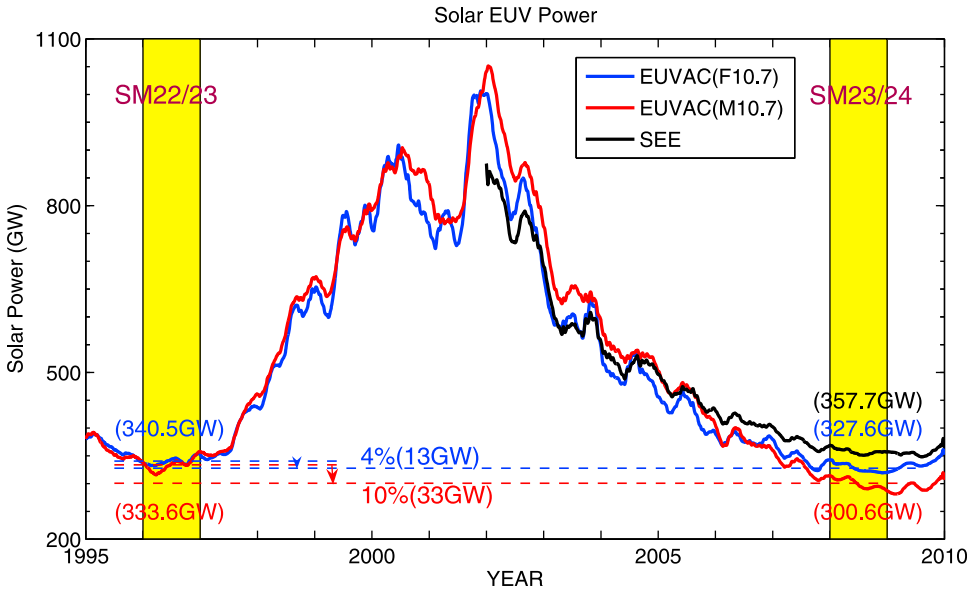

Figure 3. The same as Figure 1 but for the comparison of solar power from different sources including EUVAC driven by $F_{10.7}$ (blue), EUVAC driven by $M_{10.7}$ (red) and SEE measurements (black). The annual averages in 1996 and 2008 and the difference between them have been marked.

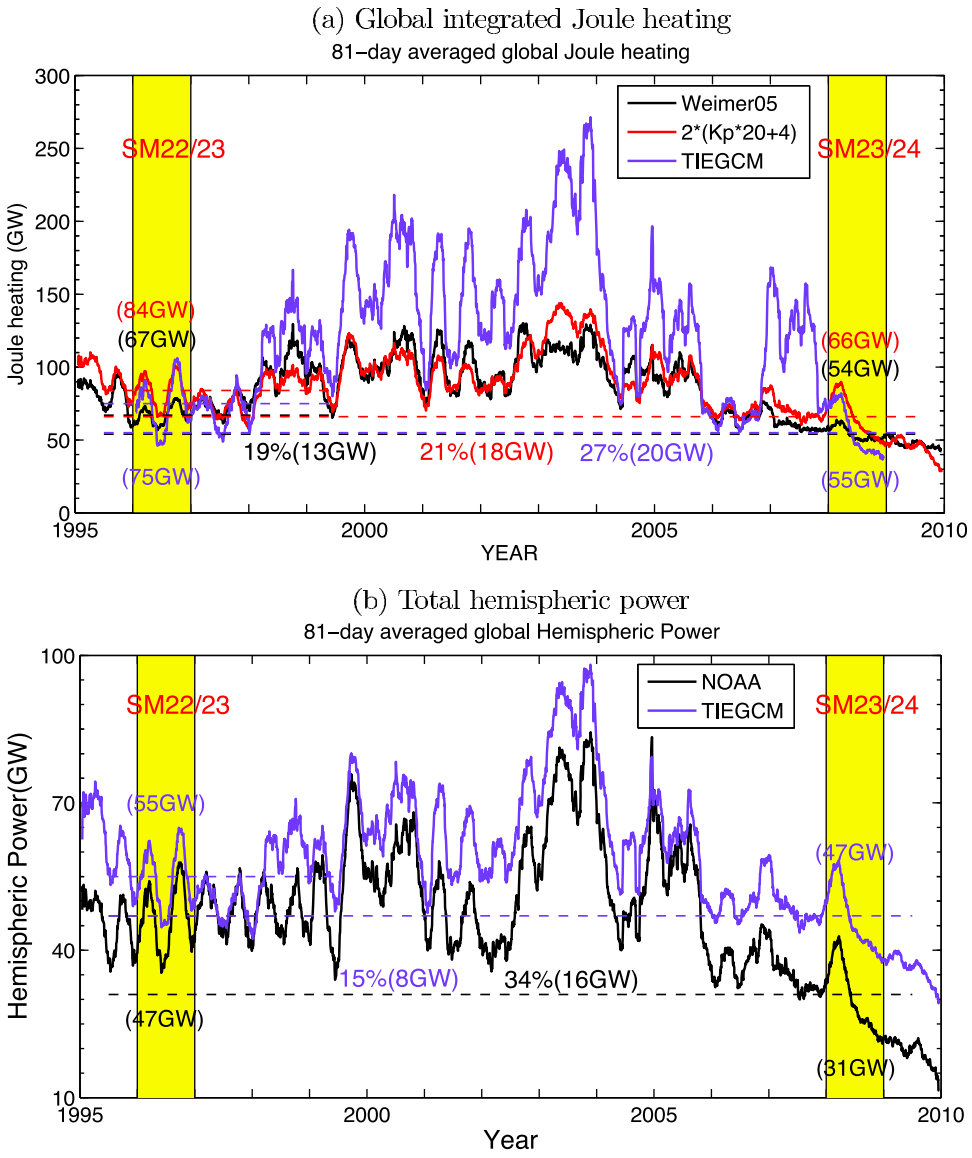

Figure 4. (a) The same as Figure 3 but for the comparison of global integrated Joule heating from different sources including W05 (black), empirical formula (red) and TIEGCM (blue). (b) The same as Figure 4a but for the comparison of the total hemispheric power from NOAA (black) and TIEGCM (blue).

normalized to 1 AU and not corrected for Sun-Earth distance, which is sufficient for this study since our main interest is the variation of yearly average.

[12] As shown in red line, the yearly average solar power in 2008 calculated from EUVAC($M_{10.7}$) was 300.6 GW, which was reduced by 33 GW (10%) compared to the value in 1996 (333.6 GW). The blue line exhibits that the solar power reduction from 1996 to 2008 calculated from EUVAC($F_{10.7}$) was close to 13 GW (4%). The change of the solar power calculated from $F_{10.7}$ index was smaller than that from $M_{10.7}$ index, which was due to the inaccuracy of $F_{10.7}$ to present the solar EUV power in the extremely low solar activity conditions during 23/24 solar minimum [*Solomon et al.*, 2011; *Chen et al.*, 2011]. As shown in *Solomon et al.* [2011], during solar minimum the $F_{10.7}$ variation was small while the solar EUV continued to decline. The measurements from SEE [*Woods et al.*, 2005] on the TIMED satellite from 2002 to 2009 have also been plotted out in black line, which in general agreed very well with the EUVAC outputs. TIMED/SEE was smaller than EUVAC in solar maximum and larger in solar minimum. Due to the way that the irradiance <27 nm was processed, the total solar power from TIMED/SEE data can be different from version to version, which may contribute to the solar-cycle dependent difference between TIMED/SEE and EUVAC. From 27 to 105 nm, TIMED/SEE is based on the EGS (EUV Grating Spectrometer) measurements, which are quite reliable [*Woods et al.*, 2005]. Unfortunately TIMED/SEE does not go back to 1996 and has no comparison between the two solar minima.

[13] The geomagnetic energy inputs into the upper atmosphere vary significantly [*Lu et al.*, 1998; *Knipp et al.*, 2005] and it is very challenging to estimate them precisely. Figure 4a shows the calculated global integrated Joule heating from W05, empirical relationship between the global Joule heating

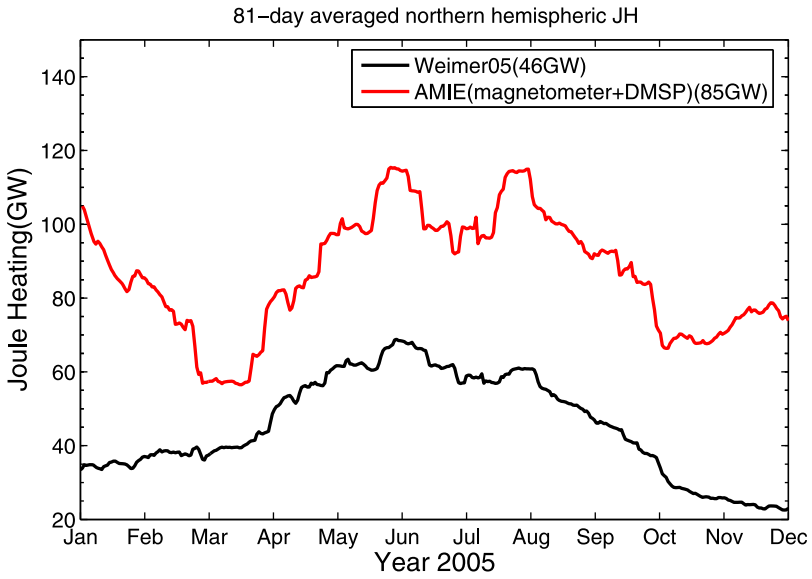

Figure 5. Comparison of the northern hemispherical integrated Joule heating between W05 and AMIE during year 2005. The annual average values from both models are indicated in the legend.

and Kp index ($JH = (20. * kp + 4) * 2.$) [*Foster et al.*, 1983] and TIEGCM. The annual average difference of Joule heating between 1996 and 2008 was 13 GW from W05, 18 GW from empirical formula, and 20 GW from TIEGCM. The estimate of Joule heating variation is limited by many processes, such as the inaccuracy of Kp index to describe the geomagnetic activity in the extreme quiet conditions during solar minimum 23/24. The Joule heating calculated from W05 is influenced by the solar wind data gaps in the OMNI data set and the limited capability of W05 to describe the electrodynamics during northward IMF conditions, such as the floor (25 kV) of the Cross Polar Cap Potential (CPCP) [*Weimer*, 2001]. The hemisphere power from NOAA measurement and TIEGCM has been compared as well. Based on TIMED/GUVI FUV data, a global auroral model has been developed [*Zhang and Paxton*, 2008] and a Kp-dependent empirical formulation of the HP has been produced. Similar formulas have been utilized in TIEGCM to calculate Hp from Kp index [*High Altitude Observatory*, 2011]. As shown in Figure 4b, HP from the empirical formulas in TIEGCM is in general higher than NOAA HP, which has also been reported in *Zhang and Paxton* [2008] and may be related to the difference of the data coverage. While the HPs are estimated from both NOAA and TIMED/GUVI satellite data, the NOAA satellite tracks just cover a tiny fraction of the auroral oval and the TIMED/GUVI swath typically covers 1/3 to 1/2 of the auroral oval [*Zhang and Paxton*, 2008]. The difference of HP between the two solar minima is 16 GW and 8 GW in NOAA measurements and TIEGCM, respectively. While the Joule heating reduction varied from 13 to 20 GW and the HP reduction also changed from 8 to 16 GW, all these sources consistently exhibited a decrease of geomagnetic energy during 23/24 solar minimum.

[14] W05 is an empirical model, which represents a climatologic distribution of the high-latitude electrodynamics. Figure 5 depicts the 81-day average of the northern hemispheric integrated Joule heating in 2005 from both W05 and the Assimilative Mapping of Ionospheric Electrodynamics (AMIE) [*Richmond and Kamide*, 1988] outputs. In AMIE run, more than 80 ground-based magnetometers and DMSP satellite electric drift measurements have been assimilated. Since the data coverage in the southern hemisphere was not as good as the northern hemisphere, only the northern hemispheric integrated Joule heating has been compared. While the difference between these two models varied with the season, W05 was consistently smaller than AMIE and the yearly average Joule heating from AMIE (85 GW) was almost two times larger than that from W05 (46 GW). If the factor of two is kept for the whole solar cycle, the Joule heating difference between 1996 and 2008 from AMIE may also double the value from W05 and reach 26 GW (2×13 GW). Certainly, more comprehensive study using the AMIE outputs during the whole solar cycle is needed to reach a general conclusion.

3.3. Influence on the Neutral Density

[15] The total energy powers just give us a rough idea of the significance to the upper atmosphere, and the energy distribution and the heating efficiency are also critical to explain the upper atmosphere variations [*Richmond*, 2010; *Deng et al.*, 2011]. Clearly the solar irradiance, Joule heating and particle precipitation have very different horizontal as well as vertical distributions [*Fuller-Rowell and Evans*, 1987; *Thayer and Semeter*, 2004; *Knipp et al.*, 2005]. Meanwhile, their heating efficiencies to the thermosphere are quite different. The heating efficiency of solar EUV is roughly 50% [*Torr et al.*, 1980], but Joule heating transfers the energy almost entirely to the neutral atmosphere [*Thayer and Semeter*, 2004; *Knipp et al.*, 2005]. Due to these differences, the effects of the solar irradiance and Joule heating on the upper atmosphere can be different even though the same amount of energy has been deposited.

[16] To investigate the relative contributions of solar EUV and geomagnetic energy to the thermospheric density reduction, some idealized simulations have been conducted. The TIEGCM does a reasonable job of tracing the satellite drag

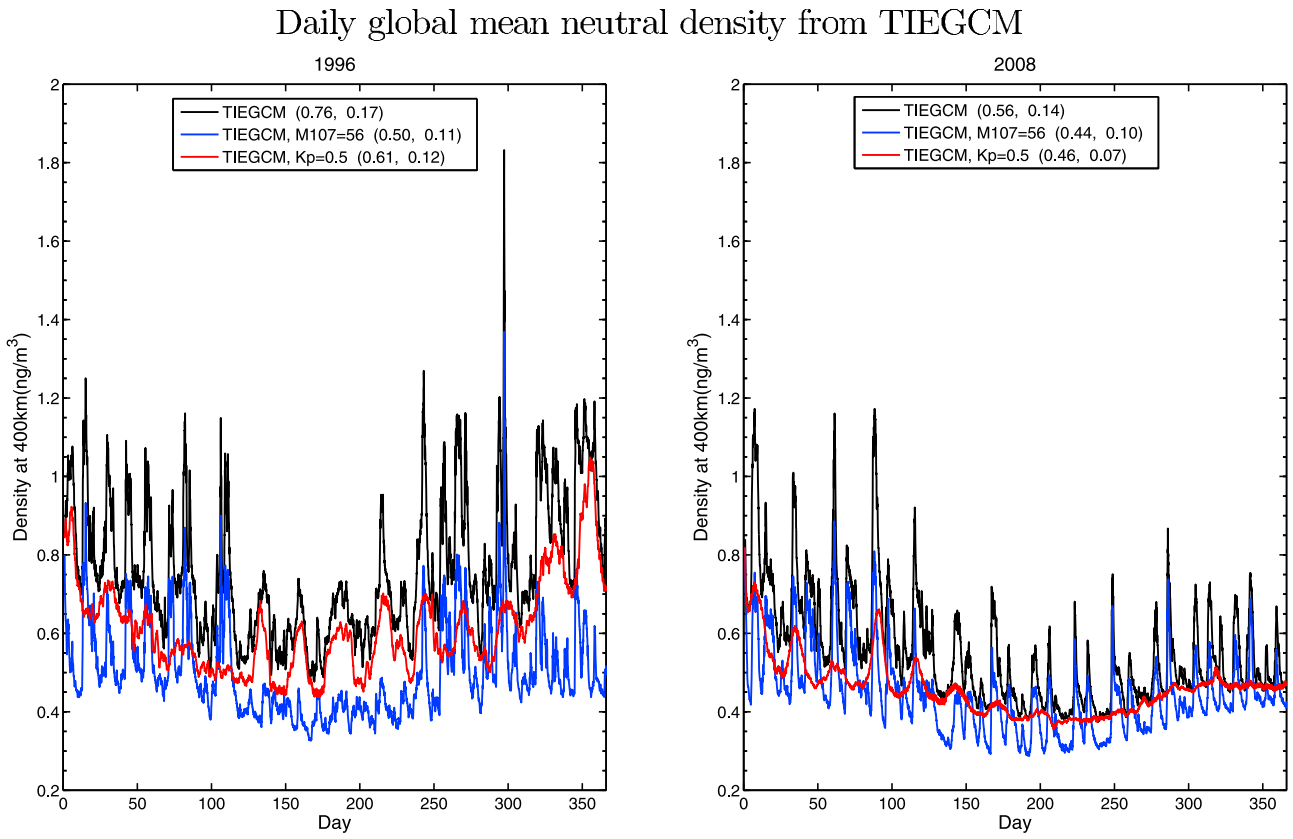

Figure 6. The TIEGCM simulated daily global mean neutral density at 400 km for (left) 1996 and (right) 2008 using $M_{10.7}$ index for the solar irradiance and Kp index for the geomagnetic energy. Black lines, both $M_{10.7}$ and Kp change with time; blue lines, $M_{10.7}$ is a constant value of 56; red lines, Kp is a constant value of 0.5. The yearly mean and standard deviation for each case have been indicated in the legend.

measurements of the neutral density [*Solomon et al.*, 2011] and has been employed for three different cases during both 1996 and 2008: case 1 with variable Kp and $M_{10.7}$ (black line in Figure 6), case 2 with a constant Kp of 0.5 and variable $M_{10.7}$ (red line in Figure 6) and case 3 with variable Kp and a constant $M_{10.7}$ of 56 (blue line in Figure 6). Case 1 (black line) represents a full simulation including the change of both geomagnetic activity and solar EUV irradiance. At 400 km altitude, the annual average density is 0.76 ng/m^3 in 1996 and 0.56 ng/m^3 in 2008. The total neutral density reduction is equal to 0.20 ng/m^3 (26%). In case 2 (red line) when Kp is a constant (0.5), the variation of the geomagnetic energy has been eliminated and the global integrated Joule heating is close to 19 GW and the total HP is 29.7 GW. The yearly average density decreased from 0.61 ng/m^3 in 1996 to 0.46 ng/m^3 in 2008 and the neutral density reduction is equal to 0.15 ng/m^3. The 0.15 ng/m^3 density change is due to the solar irradiance variation and accounts for 3/4 of the total density reduction (0.20 ng/m^3). In case 3 (blue line), $M_{10.7}$ is set to be a constant (56). The variation of the solar irradiance has been eliminated and the solar power is close to a constant (276 GW). The yearly average density is reduced from 0.50 ng/m^3 in 1996 to 0.44 ng/m^3 in 2008 at 400 km altitude and the neutral density reduction is equal to 0.06 ng/m^3. The 0.06 ng/m^3 density decrease represents the contribution of the geomagnetic energy change and is close to 1/4 of the total density change (0.20 ng/m^3). While the variation of the total geomagnetic energy (29 GW) between 1996 and 2008 is close to the variation of the solar power (33 GW), the influence of geomagnetic energy to the neutral density at 400 km is almost 3 times smaller than the solar power (0.06 ng/m^3 versus 0.15 ng/m^3). This difference is related to the energy distribution and heating efficiency. For example, the altitudinal distribution of these two energy depositions is quite different. The solar irradiance peaks around 150 km altitude and the Joule heating usually maximizes at 120 km. The effective height of solar irradiance is higher than the Joule heating. The solar irradiance is therefore more efficient to heat up the upper thermosphere at 400 km than the Joule heating [*Deng et al.*, 2011; *Huang et al.*, 2012].

[17] As illustrated in Figure 6, the temporal variation of the neutral density during these two years are quite different. In case 2 (red line) with a constant Kp, the simulation displays a repeatable 27-day cycle after DOY 120 in 1996, which is related to the Sun rotation period and corona hole structure on the Sun during that time. On contrast, in 2008 after DOY 150, the red line is very smooth with little variation, which indicates the solar power has not changed much. The standard deviation of the red lines representing neutral density variation caused by the solar irradiance variation is 0.12 and 0.07 in 1996 and 2008, respectively. Therefore, the solar irradiance in 1996 is not only averagely higher, but also more variable than that in 2008. In case 3 (blue lines), when the $M_{10.7}$ is constant, the geomagnetic energy contributes

significantly to the neutral density temporal variations, such as the neutral density spike during the geomagnetic storm on DOY 297 in 1996 and neutral density oscillation during both 1996 and 2008. The neutral density minimum happens around DOY 200 in both years, which is related to the semi-annual variation and the inter-hemispheric asymmetry. Due to the semi-annual variation, the neutral density has minima in summer and winter solstices. Meanwhile, the southern hemisphere has a much stronger semi-annual variation than the northern hemisphere and dominates the global density variation. Around DOY 200, the southern hemisphere is winter and has the lowest neutral density. The result is consistent with the CHAMP satellite measured neutral density annual variation at ~400 km during 2002–2007 [*Ercha et al.*, 2012].

4. Conclusion

[18] The solar activity during 23/24 solar-cycle minimum reached levels lower than past minima. Consequently, the record-low thermospheric density and unusual ionospheric density variation during last solar minimum have been reported, which have been mainly explained as the consequence of the anomalously low solar extreme ultraviolet (EUV) irradiance. On contrast, the variation of geomagnetic energy has been paid relatively less attention or has been treated negligible. Actually, the Sun is the ultimate energy sources for the upper atmosphere and the solar irradiance and the geomagnetic energy have been looked as the direct and indirect solar sources of energy deposition in the upper atmosphere. When the Sun activity was extremely low in 23/24 solar minimum, both direct and indirect solar sources should vary accordingly. The energy reduction in different forms is critical to explain the unusual variations in the upper atmosphere during 23/24 solar minimum. In this study, we examined the energy budget to the Earth's upper atmosphere during last solar cycle from both solar EUV irradiance and geomagnetic energy, including Joule heating and particle precipitation. The solar EUV power in 2008 calculated from the EUVAC model was reduced by 33 GW compared to 1996. The reduction of the total geomagnetic energy was close to 29 GW including 13 GW for Joule heating from W05 and 16 GW for particle precipitation from NOAA satellites measurements. While the estimations of the solar EUV power and geomagnetic energy vary from model to model, the change of the geomagnetic energy from 1996 to 2008 was comparable to the solar EUV power. The idealized simulations with TIEGCM indicate that the variations of the solar irradiance and the geomagnetic energy account for 3/4 and 1/4 of the total neutral density reduction in 2008, respectively.

[19] **Acknowledgments.** This research was supported by NSF through grant ATM0955629. The authors thank John Emmert and Kent Tobiska for the helpful suggestions. JSW was supported by NSFC (grant 40931056).

[20] Philippa Browning thanks the reviewers for their assistance in evaluating this paper.

References

Chen, Y., L. Liu, and W. Wan (2011), Does the $F_{10.7}$ index correctly describe solar EUV flux during the deep solar minimum of 2007–2009?, *J. Geophys. Res.*, *116*, A04304, doi:10.1029/2010JA016301.

Deng, Y., T. J. Fuller-Rowell, R. A. Akmaev, and A. J. Ridley (2011), Impact of the altitudinal Joule heating distribution on the thermosphere, *J. Geophys. Res.*, *116*, A05313, doi:10.1029/2010JA016019.

Emmert, J. T., and J. M. Picone (2010), Climatology of globally averaged thermospheric mass density, *J. Geophys. Res.*, *115*, A09326, doi:10.1029/2010JA015298.

Emmert, J. T., J. L. Lean, and J. M. Picone (2010), Record-low thermospheric density during the 2008 solar minimum, *Geophys. Res. Lett.*, *37*, L12102, doi:10.1029/2010GL043671.

Ercha, A., A. J. Ridley, D. Zhang, and Z. Xiao (2012), Analyzing the hemispheric asymmetry in the thermospheric density response to geomagnetic storms, *J. Geophys. Res.*, *117*, A08317, doi:10.1029/2011JA017259.

Foster, J. C., F.-P. S. Maurice, and V. J. Abreu (1983), Joule heating at high latitudes, *J. Geophys. Res.*, *88*, 4885–4897.

Fuller-Rowell, T. J., and D. Evans (1987), Height-integrated Pedersen and Hall conductivity patterns inferred from TIROS–NOAA satellite data, *J. Geophys. Res.*, *92*, 7606–7618.

Gary, J. B., R. A. Heelis, and J. P. Thayer (1995), Summary of field-aligned Poynting flux observations from DE 2, *Geophys. Res. Lett.*, *22*, 1861–1864.

Gibson, S. E., et al. (2011), The whole heliosphere interval in the context of a long and structured solar minimum: An overview from Sun to Earth, *Sol. Phys.*, *274*, 23–27, doi:10.1007/s11207–011–9921–4.

Heelis, R. A., J. K. Lowell, and R. W. Spiro (1982), A model of the high-latitude ionospheric convection pattern, *J. Geophys. Res.*, *87*, 6339–6345.

High Altitude Observatory (2011), TIEGCM V1.94 model description, Natl. Cent. for Atmos. Res., Boulder, Colo.

Huang, Y., A. D. Richmond, Y. Deng, and R. Roble (2012), Height distribution of Joule heating and its influence on the thermosphere, *J. Geophys. Res.*, *117*, A08334, doi:10.1029/2012JA017885.

Kelley, M. C., D. J. Knudsen, and J. F. Vickrey (1991), Poynting flux measurements on a satellite: A diagnostic tool for space research, *J. Geophys. Res.*, *96*, 201–207.

Knipp, D. J., W. K. Tobiska, and B. A. Emery (2004), Direct and indirect thermospheric heating sources for solar cycles 21–23, *Sol. Phys.*, *224*, 495–505, doi:10.1007/s11207–005–6393–4.

Knipp, D. J., T. Welliver, M. G. McHarg, F. K. Chun, W. K. Tobiska, and D. Evans (2005), Climatology of extreme upper atmospheric heating events, *Adv. Space Res.*, *36*, 2506–2510, doi:10.1016/j.asr.2004.02.019.

Lean, J. L., R. R. Meier, J. M. Picone, and J. T. Emmert (2011), Ionospheric total electron content: Global and hemispheric climatology, *J. Geophys. Res.*, *116*, A10318, doi:10.1029/2011JA016567.

Liu, L., Y. Chen, H. Le, V. I. Kurkin, N. M. Polekh, and C.-C. Lee (2011), The ionosphere under extremely prolonged low solar activity, *J. Geophys. Res.*, *116*, A04320, doi:10.1029/2010JA016296.

Lu, G., et al. (1998), Global energy deposition during the January 1997 magnetic cloud event, *J. Geophys. Res.*, *103*, 11,685–11,694.

Richards, P. G., J. A. Fennelly, and D. G. Torr (1994), EUVAC: A solar EUV flux model for aeronomic calculations, *J. Geophys. Res.*, *99*, 8981–8992.

Richmond, A. D. (2010), On the ionospheric application of Poynting's theorem, *J. Geophys. Res.*, *115*, A10311, doi:10.1029/2010JA015768.

Richmond, A. D., and Y. Kamide (1988), Mapping electrodynamic features of the high-latitude ionosphere from localized observations: Technique, *J. Geophys. Res.*, *93*, 5741–5759.

Richmond, A. D., E. C. Ridley, and R. G. Roble (1992), A thermosphere/ionosphere general circulation model with coupled electrodynamics, *Geophys. Res. Lett.*, *19*, 601–604.

Roble, R. G., and E. C. Ridley (1987), An auroral model for the NCAR thermospheric general circulation model (TGCM), *Ann. Geophys.*, *5A*, 369–382.

Roble, R. G., E. C. Ridley, A. D. Richmond, and R. E. Dickinson (1988), A coupled thermosphere/ionosphere general circulation model, *Geophys. Res. Lett.*, *15*, 1325–1328.

Solomon, S. C., and L. Qian (2005), Solar extreme-ultraviolet irradiance for general circulation models, *J. Geophys. Res.*, *110*, A10306, doi:10.1029/2005JA011160.

Solomon, S. C., T. N. Woods, L. V. Didkovsky, J. T. Emmert, and L. Qian (2010), Anomalously low solar extreme-ultraviolet irradiance and thermospheric density during solar minimum, *Geophys. Res. Lett.*, *37*, L16103, doi:10.1029/2010GL044468.

Solomon, S. C., L. Qian, L. V. Didkovsky, R. A. Viereck, and T. N. Woods (2011), Causes of low thermospheric density during the 2007–2009 solar minimum, *J. Geophys. Res.*, *116*, A00H07, doi:10.1029/2011JA016508.

Thayer, J. P., and J. Semeter (2004), The convergence of magnetospheric energy flux in the polar atmosphere, *J. Atmos. Sol. Terr. Phys.*, *66*, 807–824.

Torr, M., P. G. Richards, and D. G. Torr (1980), A new determination of the ultraviolet heating efficiency of the thermosphere, *J. Geophys. Res.*, *85*(A12), 6819–6826.

Viereck, R. A., L. E. Floyd, P. C. Crane, T. N. Woods, B. G. Knapp, G. Rottman, M. Weber, L. C. Puga, and M. T. DeLand (2004), A composite Mg II index spanning from 1978 to 2003, *Space Weather*, *2*, S10005, doi:10.1029/2004SW000084.

Weimer, D. R. (2001), An improved model of ionospheric electric potentials including substorm perturbations and application to the Geosphace Environment Modeling November 24, 1996, event, *J. Geophys. Res.*, *106*, 407–416.

Weimer, D. R. (2005a), Improved ionospheric electrodynamic models and application to calculating Joule heating rates, *J. Geophys. Res.*, *110*, A05306, doi:10.1029/2004JA010884.

Weimer, D. R. (2005b), Predicting surface geomagnetic variations using ionospheric electrodynamic models, *J. Geophys. Res.*, *110*, A12307, doi:10.1029/2005JA011270.

Weimer, D. R., B. R. Bowman, E. K. Sutton, and W. K. Tobiska (2011), Predicting global average thermospheric temperature changes resulting from auroral heating, *J. Geophys. Res.*, *116*, A01312, doi:10.1029/2010JA015685.

Woods, T. N., F. G. Eparvier, S. M. Bailey, P. C. Chamberlin, J. Lean, G. J. Rottman, S. C. Solomon, W. K. Tobiska, and D. L. Woodraska (2005), Solar EUV Experiment (SEE): Mission overview and first results, *J. Geophys. Res.*, *110*, A01312, doi:10.1029/2004JA010765.

Xu, W. (2011), Energy budget in the coupling processes of the solar wind, magnetosphere and ionosphere, *Chin. J. Space Sci.*, *31*(1), 1.

Zhang, Y., and L. Paxton (2008), An empirical Kp-dependent global auroral model based on TIMED/GUVI FUV data, *J. Atmos. Sol. Terr. Phys.*, *70*, 1231–1242, doi:10.1016/j.jastp.2008.03.008.